Clim Dyn
DOI 10.1007/s00382-015-2963-9

# Interaction of the recent 50 year SST trend and La Niña 2010: amplification of the Southern Annular Mode and Australian springtime rainfall

**Eun-Pa Lim[1] · Harry H. Hendon[1] · Julie M. Arblaster[1,2] · Christine Chung[1] · Aurel F. Moise[1] · Pandora Hope[1] · Griffith Young[1] · Mei Zhao[1]**

Received: 22 May 2015 / Accepted: 20 December 2015
© Springer-Verlag Berlin Heidelberg 2016

**Abstract** Australia experienced record high rainfall in austral spring 2010, which has previously been attributed to the concurrence of a strong La Niña event and a strong positive excursion of the Southern Annular Mode (SAM). In this study, we examine the role of the sea surface temperature (SST) trend over the recent 50 years, which has large warming over the tropical Indian, western Pacific and North Atlantic Oceans, in driving the extraordinary climate conditions of spring 2010, using the Australian Bureau of Meteorology coupled model seasonal forecast system. Four forecast sensitivity experiments were designed by using randomly chosen atmospheric initial conditions but with: (1) observed ocean initial conditions for 1 September 2010; (2) the same ocean initial conditions except the linear temperature trend over the period 1960–2010 was removed; (3) ocean initial conditions in which the trend was added to the climatological ocean state for 1 September; and (4) climatological ocean conditions only. A synergistic response to the La Niña SST anomalies and the SST trend was detected: the tropical rainfall anomalies were amplified over the western side of the Indo-Pacific warm-pool, which led to a significant increase of tropical upper tropospheric warming and a resultant increase of meridional temperature gradient in the Southern Hemisphere (SH) extratropics. Consequently, the SH eddy-driven jet was shifted poleward (i.e. positive phase of the SAM), which induced rainfall over subtropical Australia. Our findings highlight that the interaction of interannual anomalies and the trend may play an important role in the amplification of extreme events.

**Keywords** SST trend · La Niña 2010 · Southern Annular Mode 2010 · Australian rainfall extreme 2010

## 1 Introduction

Australia experienced its wettest spring in 2010[1] due primarily to the occurrence of a strong La Niña event in the Pacific and accompanying negative Indian Ocean Dipole (IOD; Fig. 1a) (Nicholls 2011; Hendon et al. 2014a). The associated floods resulted in loss of crops and property and increased mosquito borne disease (Anyamba et al. 2014), while the enormity of the rainfall over Australia contributed to a drop in global sea level (Fasullo et al. 2013). Impacts of this La Niña were not confined to Australia, with extreme rainfall and temperatures occurring across the globe (e.g., Trenberth and Fasullo 2012). This La Niña event occurred on the backdrop of an upward trend in sea surface temperature (SST) in the tropical Indian and western Pacific Oceans and the North Atlantic Ocean (except for the far north western Atlantic) observed since 1900 (e.g., Deser et al. 2010; Solomon and Newman 2012; Hartmann et al. 2013), thereby resulting in record or near record SSTs in parts of these basins in the second half of 2010. The extremity of weather and climate anomalies in 2010 across the globe, including Australia, has been attributed to these record SSTs (e.g., Evans and Boyer-Souchet 2012; Lyon and Dewitt 2012; Trenberth and Fasullo 2012; Hendon et al. 2014a; Ummenhofer et al. 2015). The focus of

✉ Eun-Pa Lim
e.lim@bom.gov.au

[1] Bureau of Meteorology, Melbourne, VIC 3001, Australia

[2] National Center for Atmospheric Research, Boulder, CO, USA

[1] Daily and monthly Australian rainfall data are available from 1900 (Jones et al. 2009).

Published online: 08 January 2016

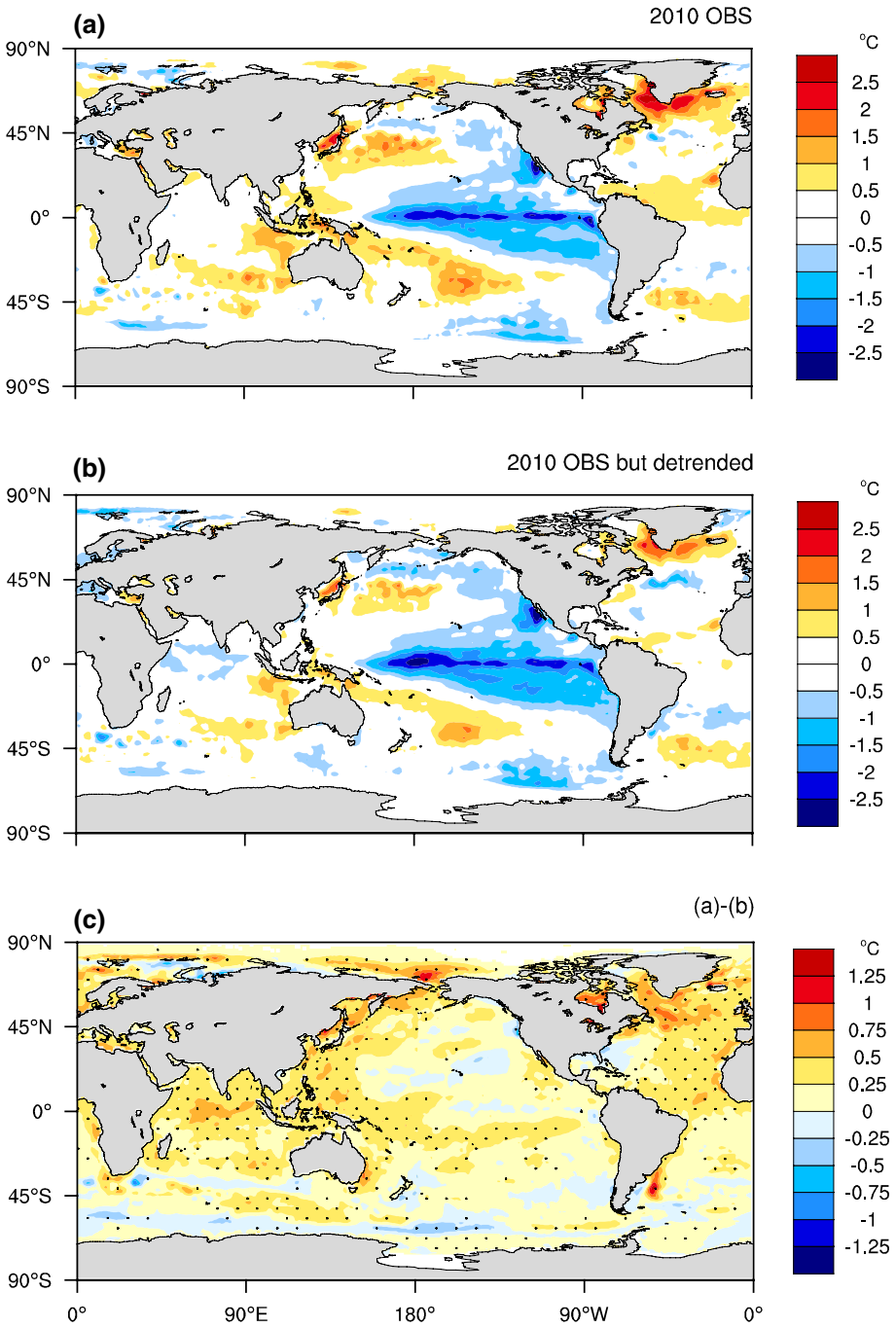


**Fig. 1** **a** 2010 September–November mean (SON) SST anomalies computed relative to the climatology for 1980–2009, using Hurrell et al. (2008)'s SST analyses; **b** as in **a** but detrended by removing the linear trend computed over 1960–2010; and **c** the SST trend in SON 2010 (i.e. **a**–**b**). The unit is °C. The *colour shading* interval is 0.5 °C for **a**, **b** and 0.25 °C for **c**. In **c** statistically significant trend at the 90 % confidence level is stippled, which is assessed by a two-tailed Student *t* test with 49 degrees of freedom

this present study is the role of the interaction of the La Niña with the underlying SST trend for promoting the record springtime rainfall in Australia 2010.

In general, La Niña induces wet conditions in Australia by the positive swing in the Southern Oscillation, whereby surface pressure drops and moisture converges over northern Australia (e.g. McBride and Nicholls 1983). The negative IOD, which typically accompanies La Niña (e.g. Meyers et al. 2007), promotes wet conditions over the south eastern part of Australia by exciting equivalent barotropic Rossby wave trains that emanate from the tropical Indian Ocean and result in cyclonic anomalies over south eastern Australia (Cai et al. 2011). Nicholls (2011) and Hendon et al. (2014a) suggested that the near-record strengths of La Niña and the negative IOD in austral spring 2010 were fundamental causes of the extraordinary wet conditions over Australia. Moreover, the Southern Annular Mode (SAM), which exhibited a near-record high positive excursion in spring 2010, was also diagnosed to have contributed to this record springtime rainfall (Hendon et al. 2014a; Lim

and Hendon 2015a). The positive phase of the SAM (also referred to as high SAM), which represents a poleward shift of the sub-polar eddy-driven jet (e.g., Thompson and Wallace 2000), acts to increase rainfall over subtropical Australia in austral spring and summer by inducing anomalous moist onshore easterly flow (Hendon et al. 2007; Meneghini et al. 2007) and upward motion (Kang et al. 2011; Hendon et al. 2014b). High SAM tends to be promoted by La Niña during austral spring/summer (e.g. Seager et al. 2003; Fogt et al. 2011; Lim et al. 2013), and high SAM was shown to be a robust response to the anomalous SST conditions of 2010, using atmosphere–ocean coupled model forecasts (Lim and Hendon 2015a).

In addition to the concurrence of La Niña, negative IOD and high SAM, Hendon et al. (2014a) inferred that 10–30 % of the record rainfall over Australia resulted from the upward trend in the SST surrounding northern Australia since 1960, consistent with earlier assessments of the impact of the SST trend estimated over the previous 30 and 50 years on extreme rainfall in early summer 2010 over north eastern Australia (Evans and Boyer-Souchet 2012; Ummenhofer et al. 2015). The SST warming trend to the north of Australia over the 50 years from 1960–2010 is part of a broad-scale warming pattern whereby the Indian, western Pacific, and North Atlantic Oceans (except for the north west of North Atlantic) have significantly warmed in the past century (e.g. Deser et al. 2010; Solomon and Newman 2012; Hartmann et al. 2013). The long-term warming trend in the tropical Indian and western Pacific SSTs observed since 1900 is in good agreement among different observational datasets (e.g. Vecchi et al. 2008; Deser et al. 2010), and it is dominantly attributed to anthropogenic forcing (Knutson et al. 2013). In contrast, it is uncertain if there is a long-term trend over the eastern Pacific, whether the sign of the trend is positive or negative (e.g. Vecchi et al. 2008; Deser et al. 2010), and how much of the eastern Pacific SST trend can be attributed to anthropogenic influences (Knutson et al. 2013).

Compo and Sardeshmukh (2010) shed some light on the uncertainties in the eastern Pacific SST trend by showing that the uncertainties are likely to stem from the SST component related to the El Niño/Southern Oscillation (ENSO). In their study, the SST components independent of ENSO, which include a large component that is likely to be a response to anthropogenic forcing, demonstrate a La Niña-like long-term trend pattern (i.e. greater warming in the west than in the east over the tropical Pacific). Solomon and Newman (2012) and Sandeep et al. (2014) demonstrated that this La Niña-like SST trend that is unrelated to ENSO is captured in various data sets. Moreover, the La Niña-like SST trend has been further strengthened recently by the cold phase of Interdecadal Pacific Oscillation after the strong El Niño of 1997–1998 (e.g. Kosaka and Xie 2013; Meehl et al. 2014; England et al. 2014; Zhao et al. 2015). Although the debate is still ongoing about the sources of the eastern Pacific SST trend and uncertainties associated with them, it is clear that the 50-year trend in SSTs from 1960 to 2010 has a somewhat "La Niña-like" spatial pattern (Fig. 1c), and this trend likely combined synergistically with the 2010 La Niña conditions and positively contributed to the record Australian springtime rainfall.

The present study is aimed at diagnosing the impact of the recent 50 year linear trend in SST on the anomalous southern hemisphere (SH) extratropical circulation and record Australian rainfall in austral spring 2010. Also, we aim to understand the underlying mechanism by which La Niña and the trend interacted so to increase rainfall over Australia, with a goal to improve our understanding of the likelihood and predictability of rainfall extremes. Our approach is to conduct a series of forecast sensitivity experiments with the Australian Bureau of Meteorology (BoM)'s dynamical seasonal climate prediction system. This system successfully predicted the extraordinary climate conditions of spring 2010 (Lim and Hendon 2015a). The configuration of the forecast model and the design of experiments are provided in Sect. 2. The observed climate conditions of spring 2010 are described in Sect. 3. Results from the forecast sensitivity experiments are presented in Sects. 4 and 5, and concluding remarks are provided in Sect. 6.

## 2 Data and methodology

### 2.1 POAMA seasonal prediction system

To identify how the linear trend in global SST contributed to the climate anomalies during La Niña 2010, in particular the extreme Australian rainfall, we run short-lead seasonal forecasts using a global coupled model with and without inclusion of the linear trend in the ocean initial conditions. Alternatively, we could have run uncoupled simulations with prescribed SSTs, which would better constrain the evolution of the SSTs to the observed (e.g., Lewis and Karoly 2015; Ummenhofer et al. 2015). However, climate in the Indo-Pacific warm pool region is sensitive to air-sea coupling especially in austral spring (e.g., Hendon et al. 2012) and so a coupled simulation will more faithfully reproduce the two-way interaction of the atmosphere and upper ocean (e.g. Lim and Hendon 2015b). A potential pitfall, of course, is that the predicted SST evolution during the coupled model forecast will not follow the observed behaviour, thereby rendering our results irrelevant. However, we will show that the predicted SSTs skilfully reproduce the major observed characteristics of the SSTs in 2010 over the course of the first 3-month forecasts.

**Table 1** Design of forecast sensitivity experiments, using high quality observed initial conditions generated by the BoM's atmosphere-land and ocean data assimilation systems (Hudson et al. 2011; Yin et al. 2011)

| Experiments | Ocean initial conditions | Atmosphere and land initial conditions |
|---|---|---|
| $CTRL_{2010}$ | 00 UTC 1 September 2010 | 00 UTC 1 September 1980–2009 (i.e. 30 different conditions for each experiment) |
| $DTR_{2010}$ | 00 UTC 1 September 2010 except the temperature trend over 1960–2010 was subtracted | |
| TR | The temperature trend over 1960–2010 added to the mean conditions of 00 UTC 1 September 1980–2009 | |
| CLIM | Mean conditions of 00 UTC 1 September 1980–2009 | |

Forecasts are initialised at 00 UTC 1 September 2010 and run for 3 months to be verified for the September–November mean of 2010

We use the Predictive Ocean and Atmosphere Model for Australia (POAMA) version 2, which is the BoM's coupled model seasonal climate prediction system (Wang et al. 2005). The atmospheric component is the BoM Atmospheric Model version 3 (BAM3; Colman et al. 2005), which has ~250 km horizontal resolution (triangular truncation T47) on 17 vertical levels (L17). The land surface scheme is a simple bucket model for soil moisture with three levels for temperature (Manabe and Holloway 1975; Hudson et al. 2011). The ocean component is the Australian Community Ocean Model version 2 (ACOM2; Schiller et al. 2002; Oke et al. 2005), which is based on the GFDL modular ocean model (MOM2; Pacanowski 1996). The ocean model has horizontal resolution of 2° in the zonal direction and 0.5° in the meridional direction in the tropics that increases to 1.5° towards the poles. ACOM2 has 25 vertical levels with 13 levels in the top 200 m. BAM3 and ACOM2 are coupled by the Ocean Atmosphere Sea Ice Soil (OASIS) software (Valke et al. 2000). Although the resolution of the POAMA system, especially of its atmosphere model, is relatively coarse compared to some other seasonal prediction systems (e.g. Shi et al. 2012), the POAMA system is capable of predicting climate extremes over Australia (e.g. Lim et al. 2009; Marshall et al. 2013; White et al. 2013; Arblaster et al. 2014; Lim and Hendon 2015a, b, Hope et al. 2015), and its performance across Australia compares favourably to other higher resolution seasonal climate forecast systems (Langford and Hendon 2013).

POAMA forecasts are initialised from observed atmosphere, land and ocean conditions that are generated by the BoM's atmosphere-land and ocean data assimilation systems (Hudson et al. 2011; Yin et al. 2011). The ozone concentration and sea-ice extents are prescribed with their climatological annual cycles. $CO_2$ is fixed at 345 ppm, which is the 1985 level and a default value used in the hindcast set. Additional model details and forecast performance of the POAMA for predicting tropical SSTs are provided in Cottrill et al. (2013) and Zhao et al. (2013). One notable bias in POAMA when predicting rainfall, is the underestimation over the continent, particularly across northern Australia in the austral warm seasons (e.g. Lim et al. 2009; Drosdowsky and Wheeler 2014). We correct for this mean bias by removing the model's lead-time dependent climatology. In general, POAMA demonstrates high forecast accuracy of 60–70 % in eastern and southern Australia in austral spring (e.g. Lim et al. 2009). Nevertheless, the reduced mean rainfall might result in reduced sensitivity to remote and local forcing.

### 2.2 Control and sensitivity experiments

The experimental protocol used here is designed to highlight the role of ocean conditions for driving the record rainfall over Australia in 2010. We do this by initialising the forecast model with different sets of ocean conditions on 1 September 2010 and then predicting the coupled climate for the following 3 months (September–October–November; SON). Our premise is that the ocean state evolves slowly, so that forecast differences between the experiments in the first 3 months can be attributed primarily to the differences in the imposed initial ocean states.

We conduct four different experiments as summarized in Table 1. For each of the three sensitivity experiments and the control experiment, a 30-member ensemble is generated by initialising the atmosphere model and its land surface scheme with 30 different states of 00 UTC 1 September from the years 1980–2009. These initial conditions are provided by the POAMA atmosphere-land initialisation scheme (Hudson et al. 2011). By initialising the atmosphere and land with randomized conditions, any predictability that stems from the realistic atmosphere/land initial states of 1 September 2010 is excluded in the forecasts and so highlights the role of the ocean state for driving the anomalous atmospheric circulation and rainfall in 2010.

The control experiment ($CTRL_{2010}$) is initialised with observed ocean conditions of 00 UTC 1 September 2010 as provided by the POAMA ocean data assimilation system (PEODAS; Yin et al. 2011). To examine the predicted climate for SON 2010 in the absence of the SST trend, the detrend experiment ($DTR_{2010}$) is conducted by initialising

**Table 2** Schematic description of experiment differences

| Abbreviation | Schematic formula | Inference |
|---|---|---|
| $CTRL_{2010}$ minus CLIM | (La Niña + SST trend + CLIM) − CLIM = La Niña + SST trend | La Niña with SST trend ($La\ Niña_{tr}$) |
| $DTR_{2010}$ minus CLIM | (La Niña + CLIM) − CLIM = La Niña | La Niña without SST trend ($La\ Niña_{dtr}$) |
| $CTRL_{2010}$ minus TR | (La Niña + SST trend + CLIM) − (SST trend + CLIM) = La Niña | La Niña without SST trend ($La\ Niña_{dtr}$) |
| $CTRL_{2010}$ minus $DTR_{2010}$ | (La Niña + SST trend + CLIM) − (La Niña + CLIM) = SST trend | SST trend that interplays with La Niña ($Trend_{LaNiña}$) |
| TR minus CLIM | (SST trend + CLIM) − CLIM = SST trend | SST trend that interplays with climatological SST ($Trend_{clim}$) |
| ($CTRL_{2010}$ minus $DTR_{2010}$) minus (TR minus CLIM) | $Trend_{LaNiña} - Trend_{clim} = La\ Niña_{tr} - La\ Niña_{dtr}$ | Nonlinearity of SST trend arising from the different background SST states (La Niña vs. climatological SST) |

POAMA with the same ocean conditions as the control experiment, but a linear trend over 1960–2010 is subtracted from the temperature field of the ocean initial conditions at each grid point of the three dimensional ocean. The temperature trend is estimated at each horizontal and vertical grid point at 00 UTC 1 September by linear least square fit over the years 1960–2010.[2] The SST trend pattern at 00 UTC 1 September 2010 is displayed in Fig. 11. To understand the individual role of the trend in the absence of the La Niña conditions of 2010, we also create a set of ocean initial conditions that consists of the temperature trend of 1960–2010 (shown in Fig. 11) added to the climatological conditions of 00 UTC 1 September over the 1980–2009 period. We refer to this as trend experiment (TR). For use as a reference, we also make forecasts initialised with climatological ocean initial conditions on 00 UTC 1 September based on the 1980–2009 period, which we refer to as CLIM. To highlight the climate response to La Niña and SST trend working together or separately, we form differences between the experiments as summarized in Table 2 and explained in the relevant text.

For verification of the SST forecasts, we use the SST analyses of Hurrell et al. (2008), which is a merged product of HadISST (Rayner et al. 2003) before 1982 and NOAA OI v2 SST (Reynolds et al. 2002) after 1982. For verification of atmospheric variables, we use winds, air temperatures, and mean sea level pressure (MSLP) from the ERA-Interim reanalysis (Dee et al. 2011), and monthly rainfall analysis from the CPC Merged Analysis of Precipitation (CMAP; Xie and Arkin 1996). Statistical significance testing of the difference of the means from two experiments is performed using a two-tailed Student *t* test, based on the 30 member ensemble forecasts of each experiment (e.g. Wilks 2005).

## 3 Observed anomalies of spring 2010

As described in detail in Hendon et al. (2014a), the observed SST anomalies during austral spring (SON) 2010 are dominated by La Niña conditions in the tropical Pacific, with strong cold anomalies in the equatorial central and eastern Pacific and warm anomalies in the western Pacific that arch poleward and eastward in a boomerang pattern (Fig. 1a). The warm anomaly extends into the eastern Indian Ocean, thereby strongly projecting onto the negative phase of the IOD. The detrended SST anomalies and the magnitude of the trend in 2010 are shown in Fig. 1b and c, respectively. The trend in SSTs is accountable for ~1/2 of the 2010 anomaly in the western Pacific and eastern Indian Oceans, but it accounts for little of the main La Niña cold anomalies in the eastern Pacific (Fig. 1a, c). Similar patterns of SST trend are found in other SST products such as HadISST and ERSST v4 (Smith et al. 2008; Huang et al. 2015) (not shown).

The sea level pressure anomalies demonstrate a strong positive Southern Oscillation (high pressure anomaly in the tropical eastern Pacific and low pressure anomaly to the north and west of Australia) and strong positive SAM (zonally uniform high pressure anomalies equatorward of 60°S and low pressure anomalies poleward of 60°S) (Fig. 2a). The tropical rainfall anomaly pattern reveals classical La Niña/negative IOD anomalies: dry across the tropical Pacific Ocean and over the western Indian Ocean; and wet over the tropical eastern Indian and far western Pacific

[2] The linear trend of ocean temperature estimated at 00 UTC 1 September, which is displayed in Fig. 11, is similar to the linear trend obtained using September–November mean data of the BoM's ocean reanalysis product as evidenced by the pattern correlation of the two SST trends being 0.8. A simple linear estimation of the temperature trend was adopted in this study, but other estimates of the ocean temperature trend have been used in studies with different purposes (e.g. Compo and Sardeshmukh 2010; Christidis et al. 2013a, b; Hope et al. 2015).

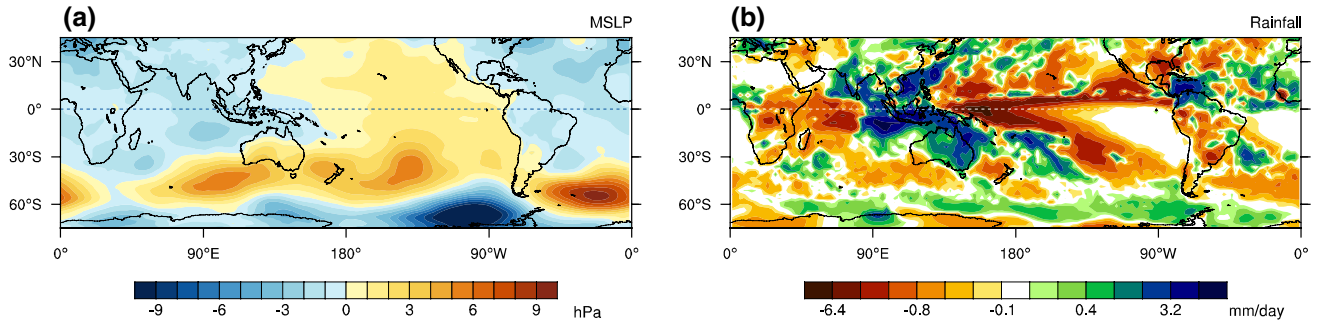


**Fig. 2** **a** Mean sea level pressure (MSLP) and **b** rainfall anomalies for SON 2010 relative to the 1980–2009 climatology, using the ERA-Interim reanalysis (Dee et al. 2011) and CMAP data (Xie and Arkin 1996), respectively. The unit is hPa and mm day$^{-1}$ for MSLP and rainfall, respectively

Oceans (Fig. 2b). Strong wet anomalies are evident over Australia, especially in the east. The extratropical rainfall anomalies in the SH show strong zonal symmetry (dry in the 30–50°S band and wet in the 50–70°S band), which reflects poleward displacement of the extratropical storm track due to the strong positive excursion of the SAM.

The vertical profile of zonal mean potential temperature and mean meridional circulation anomalies of spring 2010 shows strong warm anomalies in the midlatitudes associated with downward motion (i.e. adiabatic warming) and weak cold anomalies near the equator also associated with downward motion (i.e. diabatic cooling; Fig. 3a). The contribution of La Niña and high SAM to these anomalies is estimated by regression of the temperature and mean meridional circulation anomalies onto the inverted NIÑO3.4 SST index[3] (i.e. a measure of La Niña) and the SAM index.[4] The regression is computed over 1980–2009 and then scaled by the amplitude of the inverted NIÑO3.4 index/the SAM index of SON 2010. The observed anomaly (Fig. 3a) is thus seen to be a combination of the typical responses to La Niña conditions, with cold anomalies/sinking motion near the equator and weak warm anomalies/sinking motion in the subtropics to midlatitudes (25–40°S) (Fig. 3b), and to high SAM, with warm anomalies/sinking motion in the midlatitudes (40–50°S) and cold anomalies/upward motion in the high latitudes (60–70°S) (Fig. 3c). However, the combination of La Niña and high SAM using a multiple linear regression technique reveals that the diabatic cooling near the equator in 2010 was not as strong as would be anticipated for a La Niña event of this magnitude (Fig. 3d). There is even the appearance of positive temperature anomalies in the tropical upper troposphere (Fig. 3a). This positive temperature anomaly is likely to result from the anomalous warming due to the SST trend, which was large enough to offset the strong zonal mean cold anomaly driven by La Niña. This premise will be tested below.

## 4 Forecasts of spring 2010

### 4.1 Forecasts with and without the SST trend

The ensemble mean forecast of $CTRL_{2010}$ shown as ($CTRL_{2010}$ minus CLIM) reveals the full impact of the La Niña SST anomalies operating in conjunction with the trend in SST (Fig. 4 left panels; Table 2). The observed SST pattern of spring 2010 is skilfully predicted by $CTRL_{2010}$ (Fig. 4a), which confirms the fidelity of our experimental protocol based on short-lead coupled model forecasts. The key observed anomalies of rainfall and surface pressure described above, including the anomalous rainfall over the tropical Indian and Pacific Oceans and eastern Australia (Fig. 4c) and strong positive Southern Oscillation and positive SAM (Fig. 4b; Table 3), are also well predicted. However, the magnitude of forecast rainfall anomalies are somewhat smaller than observed, especially over the Australian continent, which could be due to the forecast model's systematic dry bias over land as discussed earlier (e.g. Lim et al. 2009; Hendon et al. 2012) but also due to the use of random atmosphere and land conditions to initialise these forecasts (Lim and Hendon 2015a).

The response to La Niña in the absence of the SST trend is assessed with ($DTR_{2010}$ minus CLIM) (Table 2). The pattern of anomalies in rainfall and surface pressure (Fig. 4 right panels) is nearly identical to the response when the trend is included (Fig. 4 left panels). That is, the strong positive phase

[3] NIÑO3.4 index $= \overline{SSTa}_{(5°S-5°N,190-240°E)}$, where SSTa indicates SST anomalies, and the overbar denotes area average.

[4] SAM index$_t = \sum_i^I \sum_j^J \lambda_{ij} MSLPa_{ijt}$, where $\boldsymbol{\lambda}$ denotes the 1st eigenvector of the Empirical Orthogonal Function (EOF) of MSLP anomalies over the domain of 25–75°S, 0–360°E for the period 1980–2009, which is displayed in Fig. 12. MSLPa indicates MSLP anomaly. i, j, and t denote longitude, latitude and time, respectively.

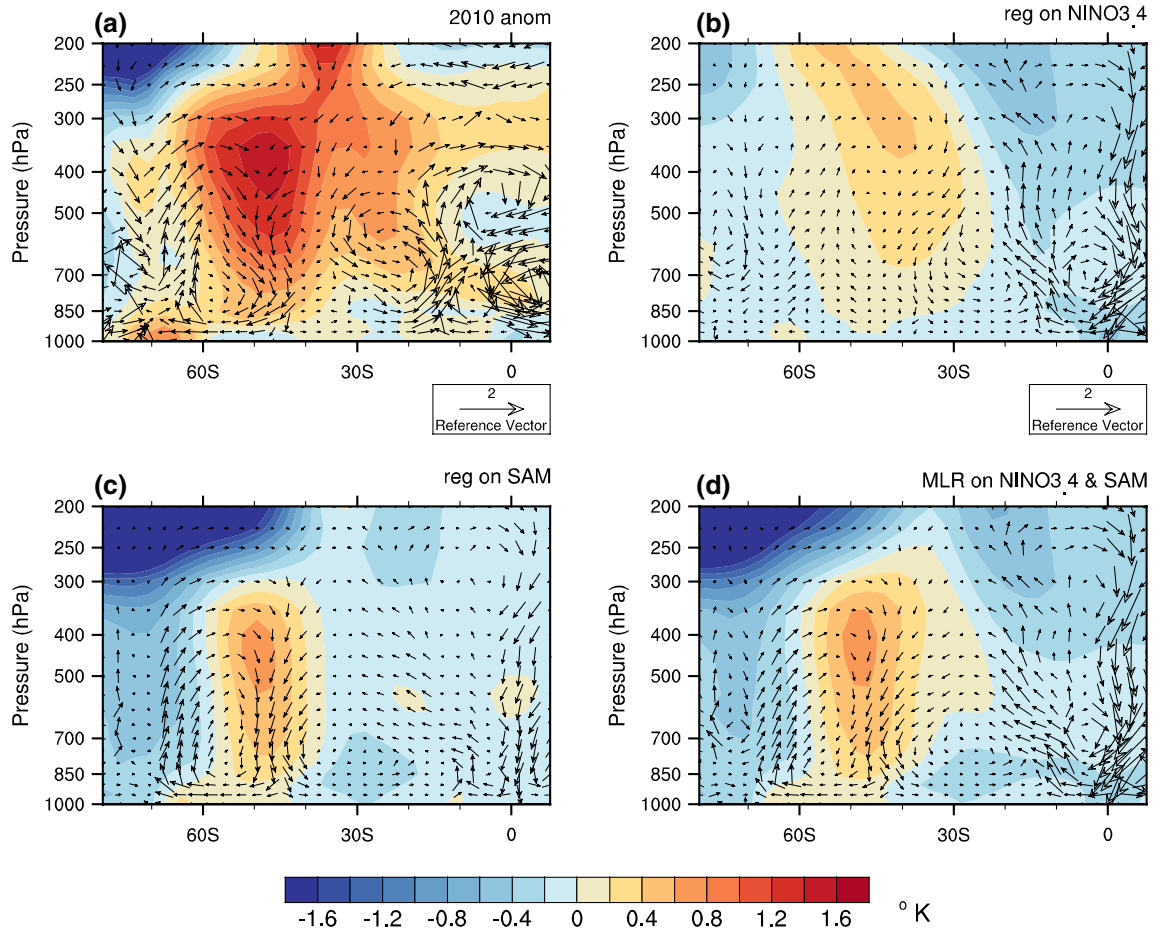


**Fig. 3** Anomalies of zonal mean potential temperature (*colour shading*) and meridional circulation (v, ω: vectors) **a** observed in SON 2010, **b** regressed on the inverted NIÑO3.4 SST index, **c** regressed on the SAM index, and **d** multiple linearly regressed (MLR) on the inverted NIÑO3.4 SST index and the SAM index. The regression coefficients were computed for the period 1980–2009 and scaled by the amplitudes of the SAM and NIÑO3.4 SST of 2010 for SON. The unit is $ms^{-1}$ and Pa $s^{-1}$ for meridional and vertical winds, respectively (vertical winds scaled by 200) and °K for temperature

of the Southern Oscillation in the tropics and the strong swing to high SAM in the SH extratropics are still apparent, as is the increased rainfall over Australia, which confirms that the primary forcing of the key circulation and rainfall anomalies in 2010 was La Niña. However, close inspection of Fig. 4 and Table 3 reveals that the rainfall anomalies over Australia and the magnitude of the SAM are reduced in the absence of the SST trend. Removal of the trend also reduces the magnitude of the negative IOD and the warm SST anomaly to the north of Australia by about 25–30 % but has little impact on the magnitude of La Niña or the Southern Oscillation (Table 3). The specific impact of the SST trend on the climate of spring 2010 is addressed below.

### 4.2 Impact of the trend

The response of the atmosphere to the SST trend can be examined by creating the difference (TR minus CLIM), referred to as $\text{Trend}_{\text{clim}}$, or by the difference ($\text{CTRL}_{2010}$ minus $\text{DTR}_{2010}$), referred to as $\text{Trend}_{\text{LaNiña}}$ (Table 2). If the system were linear, the result of $\text{Trend}_{\text{clim}}$ and $\text{Trend}_{\text{LaNiña}}$ would be equal (see the expansion of the components of these experiments in Table 2). However, if the interaction between La Niña and the trend in $\text{CTRL}_{2010}$ leads to any nonlinear response, then it will be evidenced in the difference between $\text{Trend}_{\text{LaNiña}}$ and $\text{Trend}_{\text{clim}}$.

The impact of the trend is examined first with $\text{Trend}_{\text{LaNiña}}$ (i.e. $\text{CTRL}_{2010}$ minus $\text{DTR}_{2010}$). The trend in SSTs as simulated in these experiments (Fig. 5a) matches reasonably well the observed trend (Fig. 1c): key features of the observed trend that are depicted in the experiments include maximum warming in the tropical central to eastern Indian, western Pacific and North Atlantic Oceans. Therefore, a "La Niña-like" trend pattern with the steepened west-east zonal temperature gradient in the tropical Pacific basin is reproduced in $\text{Trend}_{\text{LaNiña}}$. According to Table 3, about

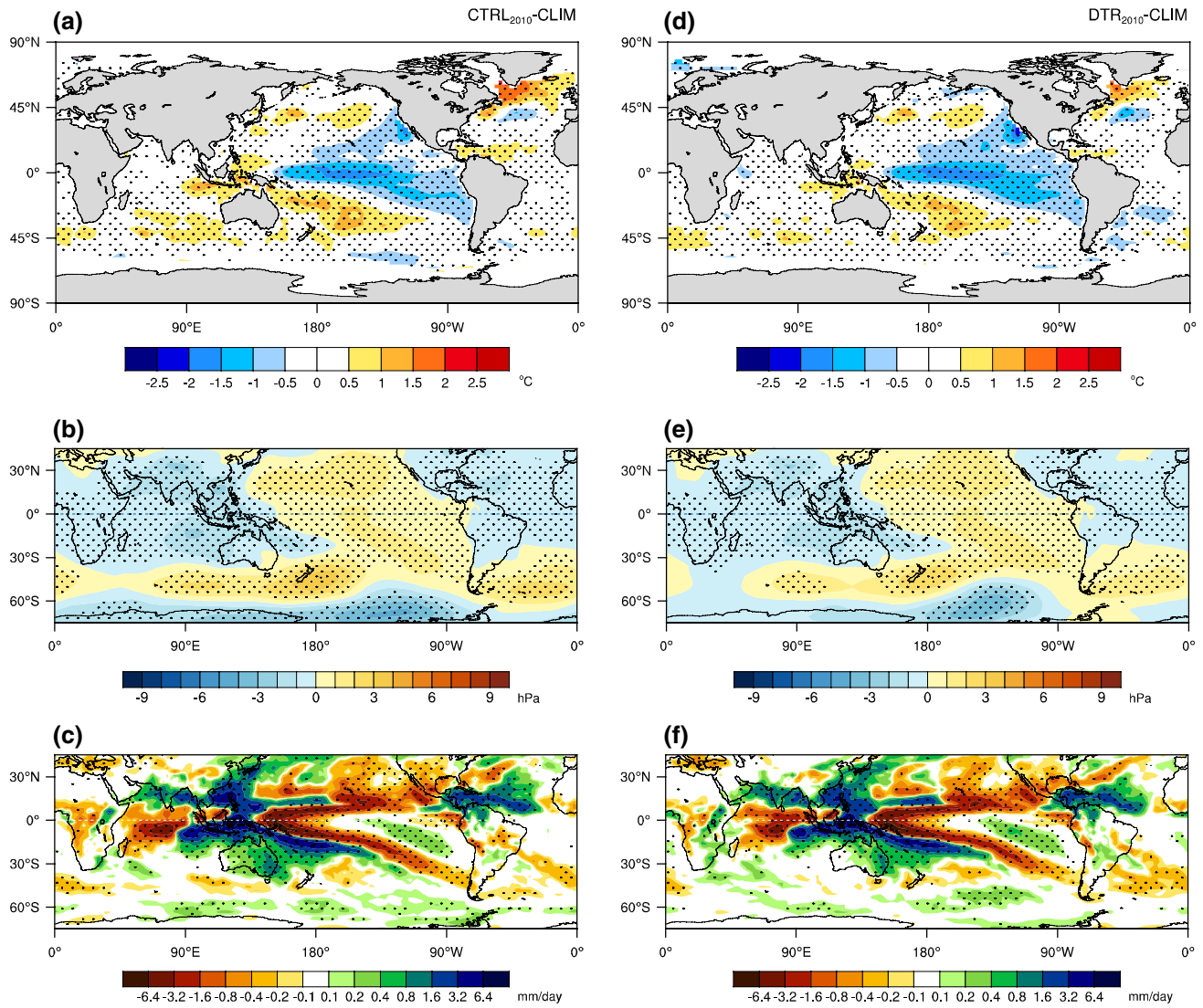


**Fig. 4** Zero lead forecasts (i.e. forecasts initialised on 1 Sep 2010 and verified for September–October–November 2010) of **a**, **d** SST, **b**, **e** MSLP, and **c**, **f** rainfall anomalies ($CTRL_{2010}$ minus CLIM) (**a**–**c** *left panels*) and ($DTR_{2010}$ minus CLIM) (**d**–**f** *right panels*) for SON 2010. Statistically significant differences at the 90 % confidence level (CL) are stippled. Statistical significance was assessed by a two sided Student *t* test based on the two sets of 30 ensemble members

30 % of the SST anomaly to the north of Australia and the negative IOD anomaly is attributed to the trend. However, we note that there is a substantial underestimation of warming in the tropical western Indian Ocean and in the Maritime Continent region in $Trend_{LaNiña}$ compared to the observed trend. In order to understand the impact of this cold bias in the forecast on the results presented in the rest of this paper, we inflated the temperature trend in the ocean initial conditions of 00 UTC 1 September 2010 by the amount of the forecast bias,[5] subtracted this inflated trend from the original ocean initial conditions, and re-ran the detrended experiment with these conditions (i.e. the initial condition difference between $CTRL_{2010}$ and this detrend experiment was made larger than that between $CTRL_{2010}$ and $DTR_{2010}$). With this bias adjustment, the warming trend in the western Pacific and the Maritime Continent region was better simulated by ~0.2 °C, but its impact on the atmosphere was not significantly different from what is shown in Fig. 5b, c (not shown).

Consistent with the positive SST anomalies due to the trend, pressures are significantly lower over the tropical-subtropical eastern Indian Ocean and the Maritime Continent region (Fig. 5b) although there is no detectable

[5] At the sea surface, this inflated temperature trend is the sum of the pattern shown in Fig. 11 (the original trend used for $DTR_{2010}$) and the pattern of Fig. 1c minus Fig. 5a (i.e. the forecast bias).

**Table 3** Climate indices from the forecast sensitivity experiments

| | sSOI | sSAMI | NIÑO3.4 index (°C) | DMI (°C) | SSTnAUI (°C) | AUS rainfall (mm/day) |
|---|---|---|---|---|---|---|
| $CTRL_{2010}$ minus CLIM (La $Niña_{tr}$) | **4.74** | **0.67** | **−1.44** | **−0.94** | **0.47** | **0.47** |
| $DTR_{2010}$ minus CLIM (La $Niña_{dtr}$) | **4.74** | **0.44** | **−1.50** | **−0.68** | **0.33** | **0.30** |
| $CTRL_{2010}$ minus $DTR_{2010}$ ($Trend_{LaNiña}$) | 0.00 | 0.23 | **0.06** | **−0.26** | **0.14** | **0.17** |
| TR-CLIM ($Trend_{clim}$) | −0.10 | −0.18 | **−0.20** | **−0.36** | **0.14** | 0.04 |

Statistically significant differences at the 90 % confidence level are bold-faced. Statistical significance was assessed by a Student *t* test based on 30 ensemble members of each of the two experiments. SST trend is represented by SST north of Australian Index (SSTnAUI), which is the areal mean of SST anomalies over 110–160°E, 0–10°S, as defined by Hendon et al. (2014a). SOI and SAM indices were normalized by the standard deviations of the ensemble spread of the 30 ensemble members of the SOI and SAM indices of the CLIM experiment

$SOI = 10 \times \frac{Pdiff - Pdiffav}{\sigma(Pdiff)}$, where Pdiff is Tahiti MSLP minus Darwin MSLP, Pdiffav is the long-term climatology of Pdiff, σ(Pdiff) is the standard deviation of Pdiff over the climatological period (http://www.bom.gov.au/climate/glossary/soi.shtml)

$DMI = \overline{SSTa}_{(10°S-10°N,50-70°E)} - \overline{SSTa}_{(10°S-eq,90-110°E)}$ (Saji et al. 1999)

$SSTnAUI = \overline{SSTa}_{(10°S-eq,110-160°E)}$ (Hendon et al. 2014a)

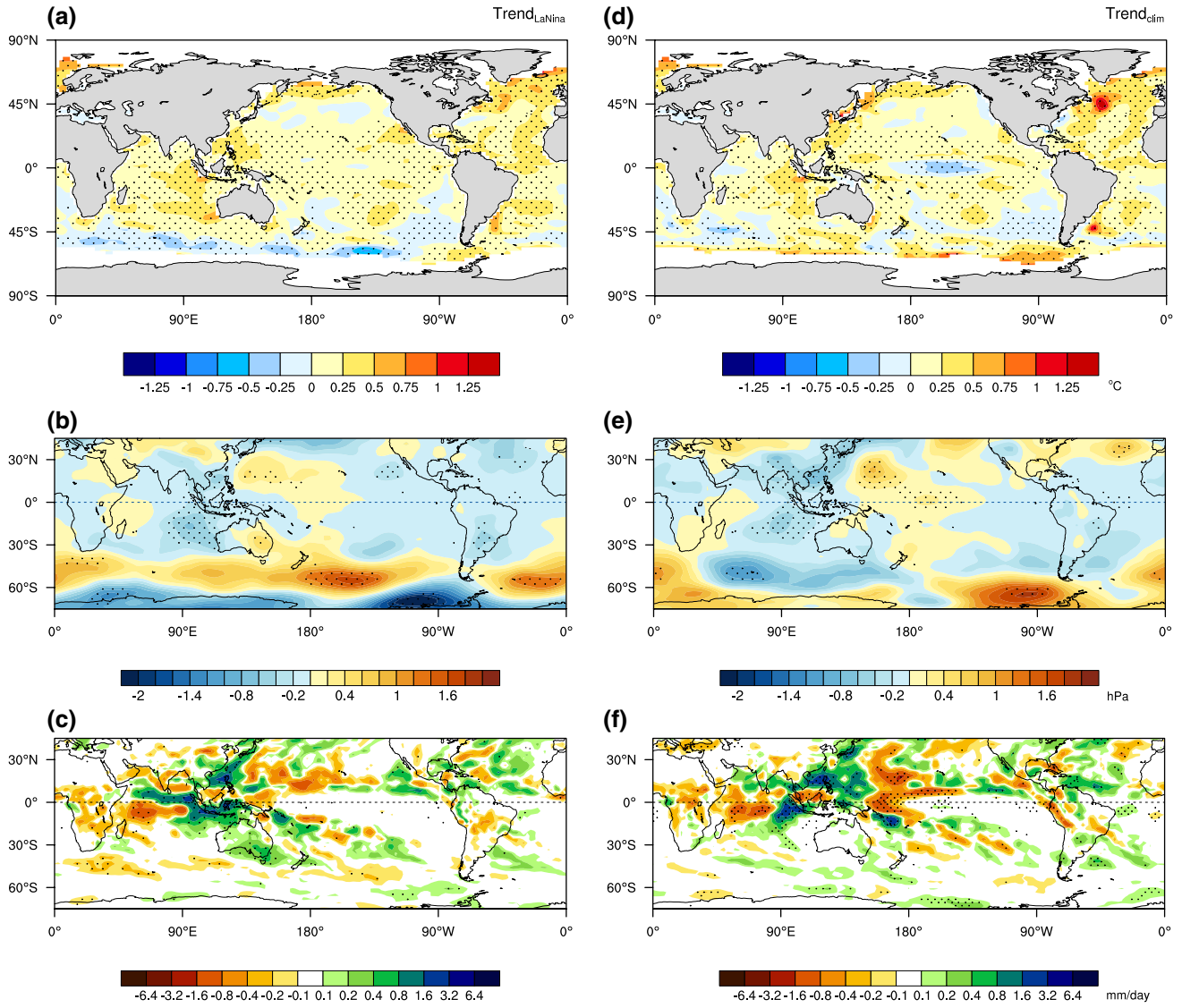


**Fig. 5** As in Fig. 4 except for **a–c** differences arising from SST trend in the presence of La Niña ($Trend_{LaNiña}$) and **d–f** differences arising from SST trend in the absence of La Niña ($Trend_{cliim}$)

difference in the Southern Oscillation (Table 3). Rainfall is increased in the regions of low pressure and high SST anomalies (Fig. 5c), with the strongest increases over the eastern Indian Ocean-Maritime Continent and the South Pacific Convergence Zone, and over southern Australia. In contrast, rainfall is decreased in the western-central Indian Ocean/Africa and western Pacific northeast of Papua New Guinea. In general, the impact of the SST trend appears to amplify the rainfall response associated with La Niña and negative IOD of 2010 (i.e. compare Figs. 5c to Fig. 4f). Also, it is interesting to note that $\text{Trend}_{\text{LaNiña}}$ results in an enhanced positive swing of the SAM and associated zonally symmetric rainfall anomalies in the extratropics (Fig. 5b, c). Much of the enhanced positive rainfall anomaly over the southern part of Australia is seen to be a part of this zonally symmetric SAM response. Based on these experiments, about 35 % of Australian areal-mean rainfall predicted for spring 2010 is driven by this SST trend (Table 3).

We next assess the impact of $\text{Trend}_{\text{clim}}$, the difference (TR minus CLIM). The overall SST pattern of $\text{Trend}_{\text{clim}}$ is similar to that of $\text{Trend}_{\text{LaNina}}$ (Fig. 5d; Table 3), which is expected as the initial condition difference between TR and CLIM is the same as that between $\text{CTRL}_{2010}$ and $\text{DTR}_{2010}$. However, there is a significant SST cooling in the tropical central Pacific in $\text{Trend}_{\text{clim}}$ likely because the atmosphere–ocean coupled process takes a slightly different path of evolution in the absence of La Niña. Furthermore, the Southern Ocean shows the opposite signed SST change in $\text{Trend}_{\text{clim}}$ compared to $\text{Trend}_{\text{LaNiña}}$, which is likely due to the very different atmospheric circulation anomalies in the SH extratropics (i.e. no evidence of a SAM-like response to $\text{Trend}_{\text{clim}}$). In regard to rainfall, the impact of the trend that operates with climatological SSTs also acts to increase rainfall in the far western Pacific and eastern Indian Oceans and decrease rainfall in the western-central Indian Ocean/Africa (Fig. 5f). However, the rainfall increase over the Maritime Continent region and to the north of Australia that is found in $\text{Trend}_{\text{LaNiña}}$ is absent in $\text{Trend}_{\text{clim}}$ (Fig. 5c, f; Table 3).

The nonlinear impact of the trend arising from the presence of La Niña (i.e. $\text{Trend}_{\text{LaNiña}} - \text{Trend}_{\text{clim}}$), which is the difference in the left hand and right hand panels in Fig. 5, is displayed in Fig. 6. These differences highlight the rainfall increase over the tropical Indian Ocean to the north of the equator, the Maritime Continent region and southern Australia and a strong signature of high SAM (Fig. 6b–d). However, this nonlinear atmospheric response to the trend does not seem to come via the difference in SST between $\text{Trend}_{\text{LaNiña}}$ and $\text{Trend}_{\text{clim}}$: the differences in tropical SSTs (Fig. 6a) are small although there is a statistically significant difference in the equatorial central Pacific, and more importantly, these differences are much smaller than the SST anomalies associated with La Niña (Fig. 4d) or the trend itself (Fig. 5a, d). Besides, if the statistically significant positive difference between $\text{Trend}_{\text{LaNiña}}$ and $\text{Trend}_{\text{clim}}$ in the equatorial central Pacific played any role in the atmosphere, it should have been to promote low SAM not high SAM (e.g. Lim et al. 2013).

The rainfall resulting from the nonlinear interaction of La Niña and the SST trend is significantly positive over the tropical eastern Indian Ocean-Maritime Continent region where the positive SST trend and La Niña anomalies add together on top of the climatological warm-pool (Fig. 6c). Outside of the tropics, the zonally symmetric rainfall changes, including the increase over south eastern Australia (Fig. 6c, d), are consistent with the additional high SAM response to this nonlinearity (Fig. 6b). The cold SST anomaly along about 50°S (Fig. 6a) is also congruent with the promotion of high SAM because a poleward shift of the westerly jet during high SAM acts to increase surface cooling due to enhanced mixing and surface heat loss (e.g. Sen Gupta and England 2007; Ciasto and Thompson 2008). We will explore how the positive SAM could be enhanced by the trend in the SSTs acting on strong La Niña by reviewing mechanisms proposed by earlier studies and by presenting our experiment results in the following section.

## 5 Mechanism for nonlinear impact of La Niña and SST trend on high SAM

### 5.1 Proposed mechanisms of tropical-extratropical interactions

Although the SAM is known to be largely driven by atmospheric internal processes (e.g. Limpasuvan and Hartmann 1999; Lorenz and Hartmann 2001), its low frequency behaviour can be driven by tropical-extratropical interactions. For instance, La Niña induces high SAM because the tropical SST anomalies act to reduce convection along the equator thereby resulting in a weakened SH subtropical jet (i.e. anomalous increase of low latitude easterlies) (e.g. Seager et al. 2003; L'Heureux and Thompson 2006; Lim et al. 2013). The weakened subtropical jet means a poleward shift of critical latitudes where the phase speeds of eddies equal background zonal wind speeds (e.g. Seager et al. 2003; Lu et al. 2008). Thus, in the upper troposphere the equatorward propagating eddies that emanate from the higher latitude baroclinic zone break poleward of their climatological location, thereby inducing an anomalous easterly acceleration in the subtropics. The induced mean-meridional circulation to balance this easterly acceleration in the subtropics results in anomalous convergence, sinking motion and warm anomalies in the midlatitudes (similar to what is displayed over 25–40°S in Fig. 3b; e.g. Seager et al. 2003). Consequently, the meridional temperature gradient

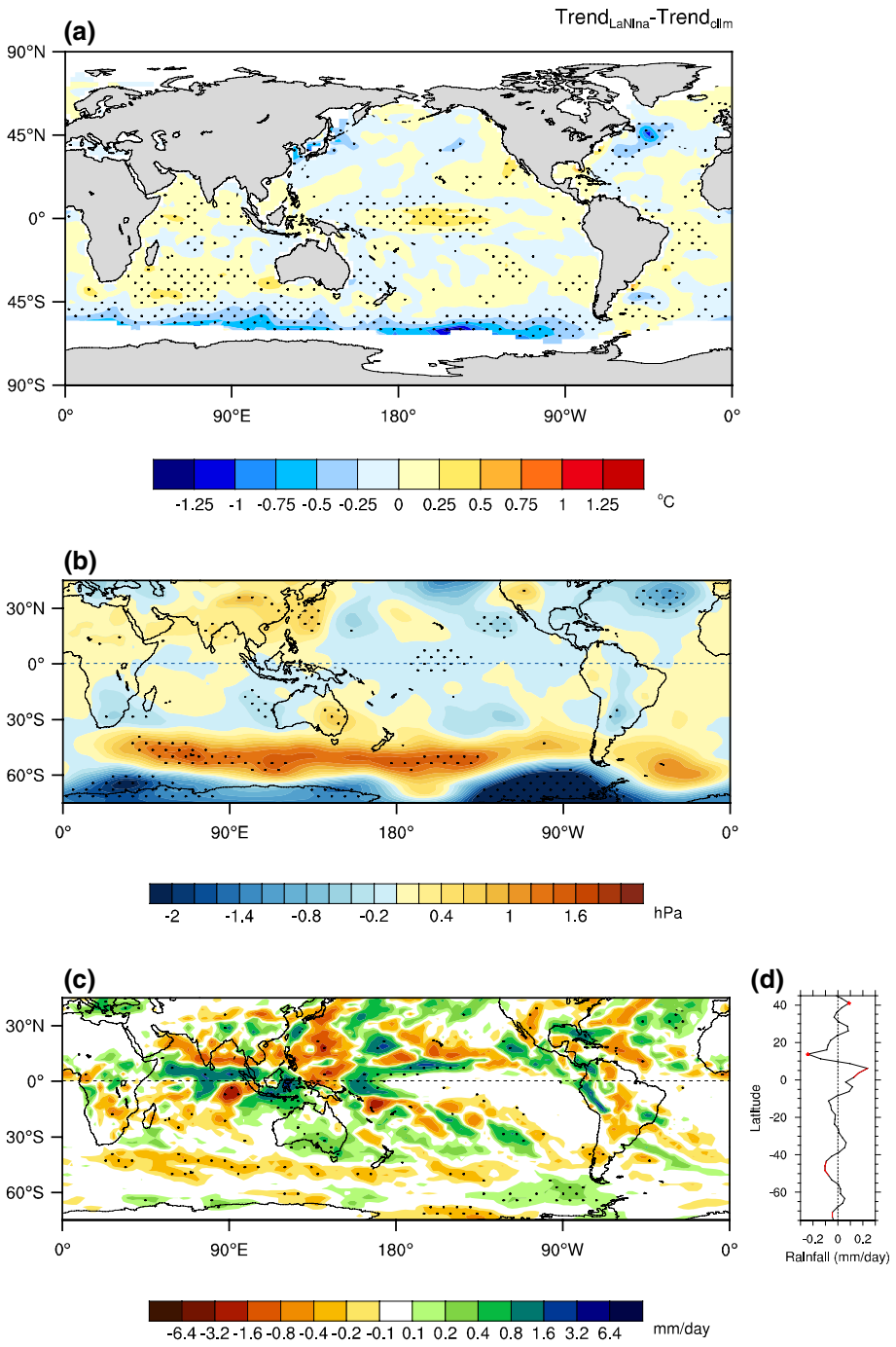


**Fig. 6** As in Fig. 4 except for differences between the two estimates of SST trend ($Trend_{LaNiña}$ minus $Trend_{clim}$; Fig. 5 *left panels* minus *right panels*). The zonal mean rainfall difference is shown in **d**, where *red* indicates differences significant at the 90 % CL

is steepened between the mid- and high latitudes, which creates strong baroclinicity for the increased growth of eddies in the high latitudes, resulting in enhanced momentum flux convergence and sustaining the poleward shift of the high latitude jet (i.e. high SAM).

High SAM is also caused by greater warming in the tropics-subtropics in the upper troposphere, which also sharpens the meridional temperature gradient between the tropics and the polar region, as shown in the future climate projections with increased greenhouse gases (e.g. Cai et al. 2003; Yin 2005; Lu et al. 2008; Lim and Simmonds 2009; Butler et al. 2010; Arblaster et al. 2011; Collins et al. 2013; Grainger et al. 2013). In particular, Lu et al. (2008) proposed that the increased extratropical temperature gradient acts to accelerate the high latitude jet and its associated eddies, and the eddies with faster phase speeds encounter their critical latitudes and break poleward of those with slower speeds. Thereby, anomalous momentum flux divergence (easterly acceleration) takes place on the subtropical side of the midlatitudes,

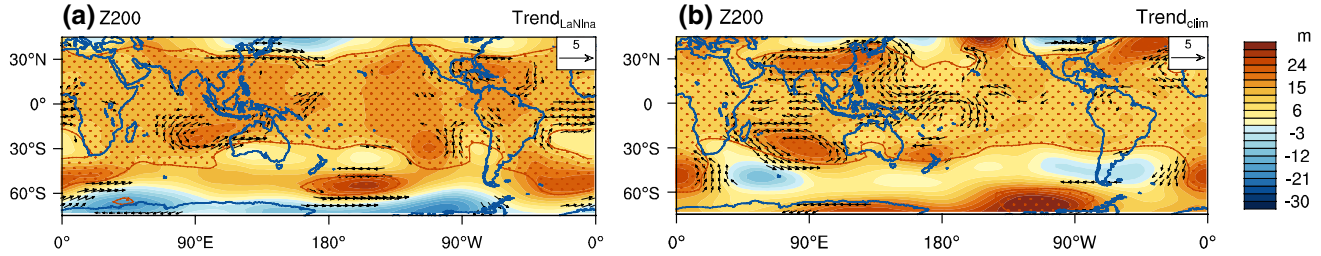


**Fig. 7** 200 hPa level geopotential height differences overlayed with horizontal wind vector differences in **a** Trend$_{LaNiña}$ and **b** Trend$_{clim}$. The unit is m and ms$^{-1}$ for geopotential height and winds, respectively. Only statistically significant difference of the winds at the 90 % CL is displayed. The *red* contour and stippling indicate statistically significant differences of geopotential heights at the 90 % CL

and anomalous sinking motion and resultant adiabatic warming are induced poleward of the maximum divergence anomaly (e.g. Hendon et al. 2014b). Then, the same chain of processes follows as for La Niña: the meridional temperature gradient in the mid-troposphere is further sharpened by the poleward shifted adiabatic warming; which would then positively feedback to the generation of eddies in the higher latitudes (anomalous momentum flux convergence) and the decay of them in the midlatitudes (anomalous momentum flux divergence); thereby supporting a poleward shift of the high latitude jet (e.g. Robinson 2006; Kidston et al. 2010).

So, what is the mechanism by which the nonlinear interaction of the SST trend with La Niña amplified high SAM in 2010 that resulted in additional rainfall over Australia?

### 5.2 Response of the atmosphere to Trend$_{LaNiña}$

In Fig. 7 the anomalous SST warming due to the trend over the tropical eastern Indian Ocean-Maritime Continent region appears to induce a Gill-type baroclinic response of the tropical circulation as evidenced by a localised anticyclonic anomaly to the west of Australia and a ridge along the equator over the Indo-Pacific warm-pool region in the upper troposphere and the accompanying opposite signed circulation anomalies at the surface in both Trend$_{LaNiña}$ and Trend$_{clim}$ (Figs. 7a, b, and 5b, e, respectively; e.g. Gill 1980). Resultant equatorial planetary waves spread the anomalous warming to the entire tropics, leading to greater upper tropospheric warming in the tropics than the extratropics (Fig. 8a, b, d, e), consistent with other studies of the temperature response to surface warming in the tropics (e.g. Stone and Carlson 1979; Gill 1980; Sobel et al. 2002; Su et al. 2003; Santer et al. 2005). Consequently, the meridional temperature gradient between the mid- and high latitudes increases in both estimates of the impact of SST trend. However, the tropical warm anomalies are significantly larger in Trend$_{LaNiña}$ likely due to the higher rainfall anomalies over the eastern Indian Ocean-Maritime Continent region in Trend$_{LaNiña}$ compared to Trend$_{clim}$ (Fig. 8a, d vs. b, e). The difference between Trend$_{LaNiña}$ and Trend$_{clim}$ (Fig. 8c, f) clearly indicates that the interaction of the SST trend with La Niña results in larger warming in the tropical upper troposphere, steeper meridional temperature gradient in the midlatitudes, and the distinctive signature of anomalous adiabatic warming and cooling associated with high SAM in the SH mid- and high latitudes, respectively.

### 5.3 Response of characteristics of eddies to La Niña and Trend$_{LaNina}$

The enhanced meridional temperature gradient due to the larger warming of the tropical upper troposphere is known to increase eddy activity at higher latitudes than usual (e.g. Murphy et al. 2002; Lim and Simmonds 2009; Butler et al. 2010) but also to increase the phase speed of the eddies emanating from the high latitude baroclinic zone (e.g. Chen et al. 2008 and Lu et al. 2008). Because faster speed eddies generated in the high latitudes reach the critical latitudes before they get to the climatological critical latitudes, there is a poleward shift of eddy breaking zone, which leads to a chain of processes that supports a poleward shift of the high latitude eddy-driven jet (i.e. high SAM) as discussed in Sect. 5.1.

On the other hand, with La Niña conditions (when the tropics are colder than normal) the occurrence of high SAM is proposed to be instigated by a poleward shift of the subtropical critical latitudes as a result of a weakening of the Hadley circulation and an increase of stationary eddy momentum flux divergence on the equatorial side of the SH subtropical jet (e.g. Seager et al. 2003; Caballero 2007; Lu et al. 2008; Lim and Hendon 2015a), rather than any change of eddy phase speed.

The changes in the behaviour and characteristics of eddies due to these two distinctive triggering mechanisms (i.e. stronger extratropical meridional temperature gradient caused by tropical warming versus a weakening of the subtropical westerlies driven by La Niña) are well demonstrated in Fig. 9, which shows the latitudinal profile of

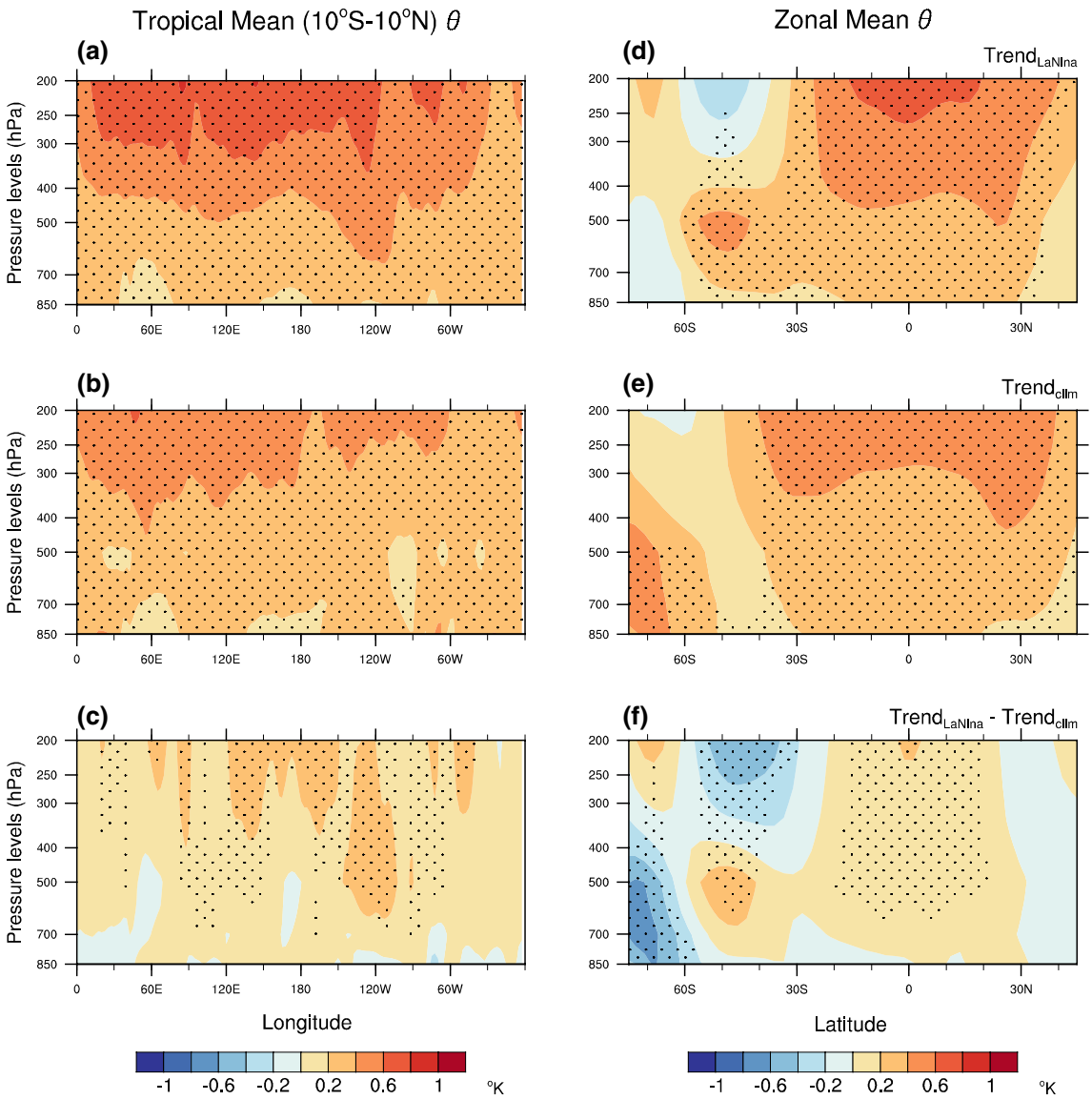


**Fig. 8** Longitude-height (**a**–**c** *left panels*) and latitude-height (**d**–**e** *right panels*) sections of potential temperature anomalies (°K) for $\text{Trend}_{\text{LaNiña}}$ (*top*) and $\text{Trend}_{\text{clim}}$ (*middle*), and their differences (*bottom*). Statistically significant changes at the 90 % CL are stippled (note that the highest model level output available in the forecast archive was the 200 hPa level)

anomalous transient eddy momentum flux convergence[6] as a function of eddy phase speed (Randel and Held 1991). The colour shading in each panel is the September–November mean momentum flux convergence simulated in the reference experiment, and the contours are the anomalies relative to that reference. We also show the mean angular velocity of zonal mean zonal winds ($u/cos\varphi$, where $\varphi$ is latitude) at 200 hPa level for the two experiments in each plot.

Firstly, $\text{DTR}_{2010}$ compared to CLIM (i.e. canonical La Niña) in Fig. 9a shows (i) weakened tropical-subtropical westerlies (black solid line compared to orange dotted line equatorward of 30°S), which indicates a poleward shift of the subtropical critical latitude; (ii) anomalous poleward shifts of the momentum flux divergence and convergence in the mid- and high latitudes, respectively

[6] $-\frac{\partial\left(\overline{[u'v']}cos^2\varphi\right)}{acos^2\varphi*\partial\varphi}$ on a spherical coordinate, where ϕ is latitude, $a$ is the earth's radius and u′, v′ are the departure of instantaneous u, v from their time means, respectively (Peixoto and Oort 1991; Seager et al. 2003). Square brackets and overbar denote zonal mean and time mean, respectively. To display eddy momentum flux convergence as a function of latitude and phase speed, we computed the space–time power spectrum by Fourier transforming daily u′, v′ relative to the September–November mean of 2010 at each latitude and then computed the meridional convergence from the space–time momentum flux cospectra at each latitude. We retained zonal wavenumbers 1–15 and smoothed in frequency with 10 passes of a 1–2–1 smoother.

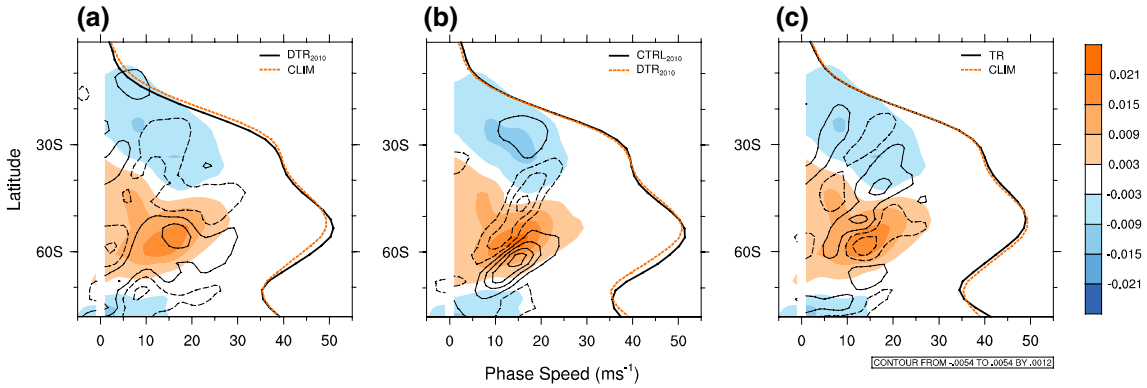


**Fig. 9** Phase speed spectra of transient eddy momentum flux convergence (*colour shadings* and *contours*) overlayed with angular velocity of zonal mean zonal wind ($u/\cos\phi$) at the 200 hPa level (*orange dotted colour line* and *black solid line*). *Contours* show the difference of momentum flux convergence between **a** $DTR_{2010}$ and CLIM, **b** $CTRL_{2010}$ and $DTR_{2010}$, and **c** TR and CLIM, respectively. *Colour shadings* show mean momentum flux convergence of the reference experiment in each case. *Colour shading* interval is 0.006 $ms^{-1}$ $day^{-1}$. Contour interval is 0.0012 $ms^{-1}$ $day^{-1}$ with first contour at $\pm 0.0006$ $ms^{-1}$ $day^{-1}$, and positive and negative values are shown with *solid* and *dashed lines*, respectively

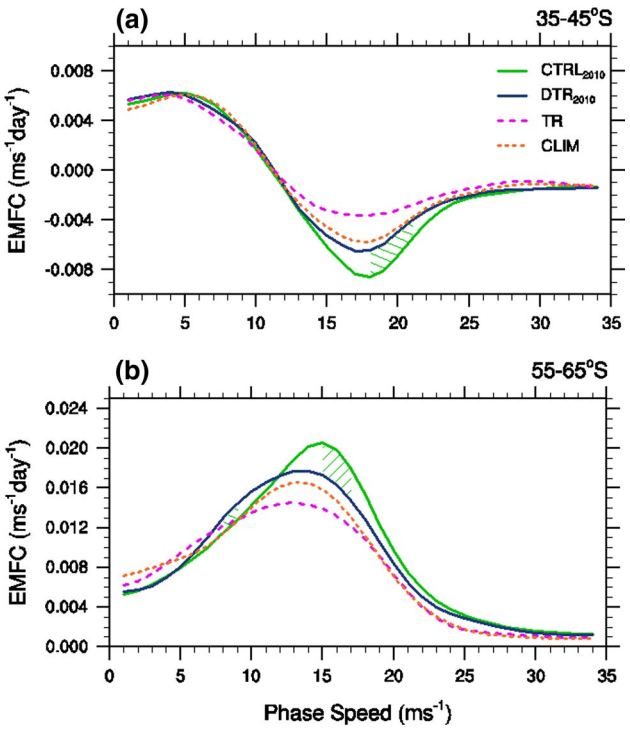


**Fig. 10** Transient eddy momentum flux convergence averaged over **a** 35–45°S and **b** 55–65°S. *Green* colored hatching indicates that the difference between $CTRL_{2010}$ and $DTR_{2010}$ at given phase speed is statistically significant at the 90 % CL (there is no statistically significant difference between TR and CLIM or between $DTR_{2010}$ and CLIM at the 90 % CL in the displayed range of phase speed in the two latitude bands)

(contours compared to colour shadings); and (iii) the resultant strengthening and poleward shift of the high latitude jet (black solid line compared to orange dotted line poleward of 45°S). These features are consistent with the processes discussed in Sect. 5.1 regarding the promotion of high SAM by La Niña. Figure 10 displays the momentum flux convergence averaged over 55–65°S and 35–45°S that represent the eddy generation and break regions, respectively. The blue solid lines of $DTR_{2010}$ compared to the orange dotted lines of CLIM confirm that the anomalous increases of momentum flux convergence in the high latitudes and momentum flux divergence in the midlatitudes during the La Niña event of 2010 occur with no obvious change in eddy phase speed.

We next compare the changes in eddy characteristics for $CTRL_{2010}$ compared to $DTR_{2010}$ (i.e. $Trend_{LaNiña}$; Fig. 9b). The SST trend with La Niña also acts to increase the momentum flux convergence at higher latitudes but the anomalous momentum flux divergence is concentrated poleward of 30°S. Hence, the zonal mean zonal wind shifts poleward in the high latitudes, but there is little change in the subtropics. Importantly, the anomalous momentum flux convergence at the high latitudes is associated with a clear shift towards faster eddy phase speeds. Figure 10 confirms that when the SST trend and La Niña are both present, the enhanced momentum flux convergence in the high latitudes and increased momentum flux divergence in the midlatitudes are due to the increased activity of eddies with higher phase speeds (green lines of $CTRL_{2010}$ compared to blue lines of $DTR_{2010}$/orange lines of CLIM). Consequently, the mechanism that links warming of the tropical upper troposphere to the amplification of the positive SAM when the SST trend operates in conjunction with La Niña appears to be via the generation of faster speed eddies in the higher latitudes. This mechanism is similar to that proposed by Chen et al. (2008) and Lu et al. (2008) to explain the poleward shift of the eddy-driven jet in response to increasing greenhouse gases.

On the other hand, the impact of the SST trend added to the climatological SSTs ($Trend_{clim}$) on the momentum flux convergence/divergence and eddy characteristics is very different from that of the trend interacting with La Niña ($Trend_{LaNiña}$) despite the similar magnitude and pattern of SST trend forcing (Figs. 9c, 10). There is no clear change in the upper level zonal mean zonal winds (Fig. 9c). Anomalous decreases of momentum flux convergence at the high latitudes rather indicate weaker eddy activity (Figs. 9c, 10), which is also consistent with the decreased meridional temperature gradient in the polar region shown in Fig. 8e.

In summary, the role of the trend in the SSTs for the atmospheric circulation is highly dependent on the SST conditions the SST trend interplays with. In the case considered here, SST anomalies associated with La Niña in the tropical eastern Indian to western Pacific Ocean are positive and so build on top of the warm anomalies there due to the warming trend and the presence of the climatological Indo-Pacific warm pool. Enhanced diabatic heating in these regions promotes an enhanced positive SAM response via steepening of the equator to pole temperature gradient so generating eddies with faster phase speeds in the high latitudes that promotes a poleward shifted jet (i.e. high SAM). Increased rainfall in the subtropical regions, including subtropical Australia, is then induced (e.g. Hendon et al. 2014b).

## 6 Concluding remarks

The austral spring climate of 2010 was extraordinary due to large excursions of the leading modes of climate variability in both the tropics (i.e. strong La Niña, negative IOD and positive Southern Oscillation) and the SH extratropics (i.e. strong positive excursion of the SAM), which together contributed to record high Australian rainfall. A long-term trend in tropical SST was shown to have played an important role for the amplification of the Australian climate response to these naturally occurring phenomena.

We showed that SST trend over the recent 50 years working together with the strong La Niña of spring 2010 significantly strengthened the warm SST anomalies over the tropical eastern Indian and western Pacific Oceans, thereby amplifying the tropical rainfall anomalies related to the strong La Niña. The associated diabatic heating acted as an important source for equatorial planetary waves that rapidly spread the warming in the upper troposphere throughout the entire tropics. This warming in the tropics steepened the meridional temperature gradient in the SH extratropics, and consequently, more eddies were generated in the higher latitudes, and their phase speed increased, inducing a poleward shift of the eddy-driven jet. Therefore, the SST trend during the La Niña of spring 2010 appears to have strengthened the positive SAM beyond what typically occurs with La Niña. This mechanism of amplification of high SAM by the SST trend interacting with La Niña is similar to the proposed mechanism by which increasing greenhouse gases will promote high SAM (e.g. Chen et al. 2008; Lu et al. 2008). In contrast, when the same SST trend was added to the climatological SSTs, a weaker atmospheric response was generated and its teleconnection pattern to the SH extratropics was very different. Its impact on Australian rainfall was also not significant.

A major caveat of these findings is that it is based on one model, and the forecast SST trend does not reproduce all the details of the observed trend. In considering uncertainties arising from these factors, it is encouraging to see that the main results are in good agreement with those of Kumar et al. (2010) who compared the La Niña events of the 1980s–2000s to those of the 1950s–1970s using observational data, which is another way to detect the impact of the SST trend operating with La Niña. They also conducted atmospheric general circulation model experiments (AMIP experiments) forced with the La Niña SSTs of the earlier epoch versus the later epoch and with the SST trend added to the climatological SSTs, which are comparable to our $DTR_{2010}$, $CTRL_{2010}$ and TR experiments, respectively. Similar to our results, Kumar et al. (2010) showed large positive anomalies of 200 hPa level geopotential height over the Maritime Continent and tropical Indian Ocean region and zonally symmetric height anomalies of high SAM in the SH extratropics as robust responses to the SST trend working together with La Niña. Furthermore, they showed that the atmospheric response over the SH extratropics to the SST trend was in a stark contrast when the same SST trend was added to the climatological SSTs. Therefore, amplification of high SAM by the SST trend interacting with La Niña is unlikely to be just an artefact of the model used in this study or result from errors in the forecast SST trend.

It is appropriate to be reminded here that the mechanism in this study results from the increased west-east gradient of SST in the tropical Pacific due to La Niña of 2010 and the "La Niña-like" SST trend estimated over the past 50 years from 1960 to 2010. Whereas, SST may trend towards a weakened SST zonal gradient (i.e. "El Niño-like" SST trend) in a future climate with increasing greenhouse gases (e.g. Xie et al. 2010; Collins et al. 2013) although there exists a large degree of uncertainty stemming from various errors in coupled climate models in capturing characteristics of dominant modes of tropical SST variability in interannual to multi-decadal time scales (e.g. Deser et al. 2012; England et al. 2014; Bellenger et al. 2014; Rashid and Hirst 2015; Kociuba and Power 2015; Luo et al. 2015). How this El Niño-like SST trend would interact with La Niña and how this combination would affect the SH extratropical circulation and Australian rainfall extremes will be another interesting topic to pursue in a future study.

A key message of our study is that whether developing naturally due to internal multi-decadal variability or being forced by anthropogenic climate change, the SST trend could play an important role in the amplification of extreme conditions caused by interannual climate variability. This highlights our need to better understand and simulate multi-year to decadal climate variability and an anthropogenically forced long-term trend and their interactions with ENSO to advance our capability to make climate predictions and projection of future climate extremes.

**Acknowledgments** This study is supported by the Victorian Climate Initiative and the Australian Climate Change Science Program. Dr Julie Arblaster is partially supported by the Regional and Global Climate Modeling Program (RGCM) of the U.S. Department of Energy's Office of Biological & Environmental Research (BER) Cooperative Agreement # DE-FC02-97ER62402. We are grateful to Dr Guo Liu for technical support to run the forecast experiments and to Drs Matthew Wheeler and Wasyl Drosdowsky and two anonymous reviewers for providing valuable comments on the manuscript. The NCAR Command Language (NCL 2014) was used for data analysis and visualization of the results.

## Appendix

See Figs. 11 and 12.

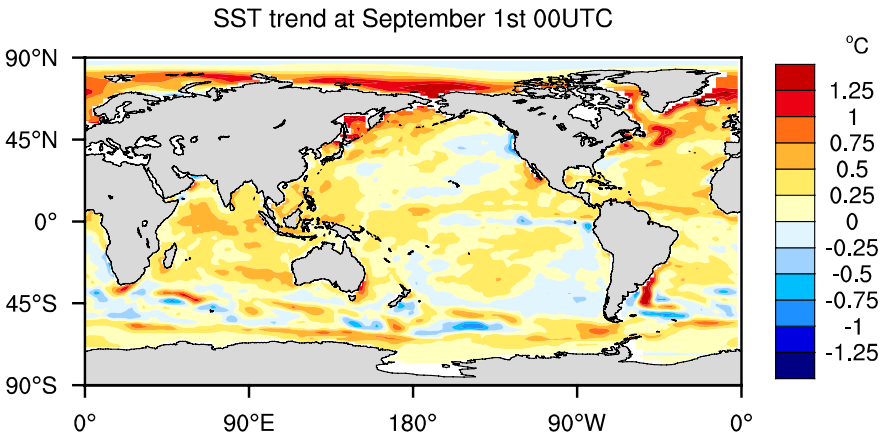


**Fig. 11** The observed SST trend estimated from September 1st 00 UTC conditions over 1960–2010, using the ocean reanalysis set generated from PEODAS (Yin et al. 2011). This pattern has 0.65 correlation with the observed SON trend pattern shown in Fig. 1c over the low latitudes of 20°S–20°N and 0.51 correlation over the globe

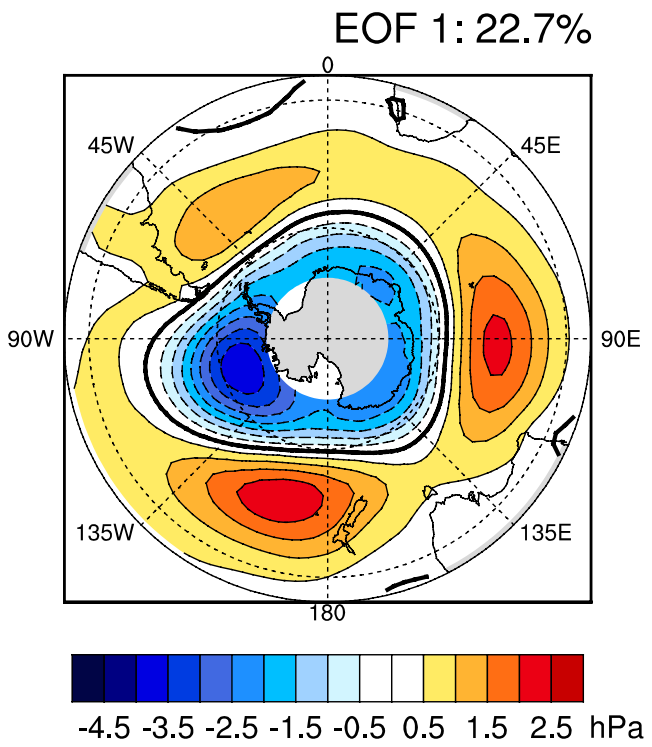


**Fig. 12** ERA-Interim reanalysis monthly MSLP anomalies regressed onto the standardized time series of the 1st mode of the EOF analysis of monthly mean MSLP anomalies, which is used as the SAM index in this study. The EOF analysis was performed on the MSLP anomalies weighted by cosine latitude over the domain of 20–75°S in the period of 1980–2009. The pattern shows the positive phase of SAM (high SAM), and the explained variance of this mode is indicated in the *top right corner* of the figure (taken from Lim and Hendon 2015a, their Fig. 2)

## References


Anyamba A, Small JL, Britch SC, Tucker CJ, Pak EW, Reynolds CA, Crutchfield J, Linthicum KJ (2014) Recent weather extremes and impacts on agricultural production and vector-borne disease outbreak patterns. PLoS ONE 9(3):e92538. doi:10.1371/journal.pone.0092538

Arblaster JM, Meehl GA, Karoly DJ (2011) Future climate change in the Southern Hemisphere: competing effects of ozone and greenhouse gases. Geophys Res Lett 38:L02701. doi:10.1029/2010GL045384

Arblaster JM, Lim E-P, Hendon HH, Trewin BC, Wheeler MC, Liu G, Braganza K (2014) Understanding Australia's hottest September on record. Bull Am Meteorol Soc 95(9):S37–S41

Bellenger H, Guilyardi E, Leloup J, Lengaigne M, Vialard J (2014) ENSO representation in climate models: from CMIP3 to CMIP5. Clim Dyn 42:1999–2018

Butler AH, Thompson DWJ, Heikes R (2010) The steady-state atmospheric circulation response to climate change-like thermal forcings in a simple general circulation model. J Clim 23:3474–3496

Caballero R (2007) Role of eddies in the interannual variability of Hadley cell strength. Geophys Res Lett 34:L22705. doi:10.1029/2007GL030971

Cai W, Whetton PH, Karoly DJ (2003) The response of the Antarctic Oscillation to increasing and stabilized atmospheric $CO_2$. J Clim 16:1525–1538

Cai W, Rensch PV, Cowan T, Hendon HH (2011) Teleconnection pathways for ENSO and the IOD and the mechanism for impacts on Australian rainfall. J Clim 24:3910–3923. doi:10.1175/2011JCLI4129.1

Chen G, Lu J, Frierson DMW (2008) Phase speed spectra and the latitude of surface westerlies: interannual variability and global warming trend. J Clim 21:5942–5959

Christidis N, Stott PA, Karoly DJ, Ciavarella A (2013a) An attribution study of the heavy rainfall over Eastern Australia in March 2012, edited by Peterson TC, Hoerling MP, Stott PA, Herring SC. Bull Am Meteorol Soc 94(9):S58–S61

Christidis N, Stott PA, Scaife AA, Arribas A, Jones GS, Copsey D, Knight JR, Tennant WJ (2013b) A new HadGEM3-A-based system for attribution of weather- and climate-related extreme events. J Clim 26:2756–2783. doi:10.1175/JCLI-D-12-00169.1

Ciasto LM, Thompson DWJ (2008) Observations of large-scale ocean-atmosphere interaction in the Southern Hemisphere. J Clim 21:1244–1259

NCL cited 2014: NCAR command language, Version 6.2.1. UCAR/NCAR/CISL/VETS. doi:10.5065/D6WD3XH5

Collins M, Knutti R, Arblaster J, Dufresne J-L, Fichefet T, Friedlingstein P, Gao X, Gutowski WJ, Johns T, Krinner G, Shongwe M, Tebaldi C, Weaver AJ, Wehner M (2013) Long-term climate change: projections, commitments and irreversibility. In: Stocker TF, Qin D, Plattner G-K, Tignor M, Allen SK, Boschung J, Nauels A, Xia Y, Bex V, Midgley PM (eds) Climate change 2013: the physical science basis. Contribution of working group I to the fifth assessment report of the intergovernmental panel on climate change. Cambridge University Press, Cambridge, pp 1029–1136. doi:10.1017/CBO9781107415324.024

Colman R, Deschamps L, Naughton M, Rikus L, Sulaiman A, Puri K, Roff G, Sun Z, Embery G (2005) BMRC atmospheric model (BAM) version 3.0: comparison with mean climatology. BMRC research report no. 108, Bureau of Meteorology Research Centre, 32 pp. http://www.bom.gov.au/bmrc/pubs/researchreports/researchreports.htm

Compo GP, Sardeshmukh PD (2010) Removing ENSO-related variations from the climate record. J Clim 23:1957–1978

Cottrill A, Hendon HH et al (2013) Seasonal forecasting in the Pacific using the coupled model POAMA-2. Weather Forecast 28:668–680

Dee DP, Uppala SM, Simmons AJ, Berrisford P, Poli P, Kobayashi S, Andrae U, Balmaseda MA, Balsamo G, Bauer P, Bechtold P, Beljaars ACM, van de Berg L, Bidlot J, Bormann N, Delsol C, Dragani R, Fuentes M, Geer AJ, Haimberger L, Healy SB, Hersbach H, Hólm EV, Isaksen L, Kållberg P, Köhler M, Matricardi M, McNally AP, Monge-Sanz BM, Morcrette J-J, Park B-K, Peubey C, de Rosnay P, Tavolato C, Thépaut J-N, Vitart F (2011) The ERA-Interim reanalysis: configuration and performance of the data assimilation system. Q J R Meteorol Soc 137:553–597. doi:10.1002/qj.828

Deser C, Phillips AS, Alexander MA (2010) Twentieth century tropical sea surface temperature trends revisited. Geophys Res Lett 37:L10701. doi:10.1029/2010GL043321

Deser C, Phillips Adam S, Tomas Robert A, Okumura Yuko M, Alexander Michael A, Capotondi Antonietta, Scott James D, Kwon Young-Oh, Ohba Masamichi (2012) ENSO and pacific decadal variability in the community climate system model version 4. J Clim 25:2622–2651

Drosdowsky W, Wheeler MC (2014) Predicting the onset of the north Australian wet season with the POAMA dynamical prediction system. Weather Forecast 29:150–161

England MH, McGregor S, Spence P, Meehl GA, Timmermann A, Cai W, Sen Gupta A, McPhaden MJ, Purich A, Santoso A (2014) Recent intensification of wind-driven circulation in the Pacific and the ongoing warming hiatus. Nat Clim Change 4:222–227

Evans JP, Boyer-Souchet I (2012) Local sea surface temperatures add to extreme precipitation in northeast Australia during La Niña. Geophys Res Lett 39:L10803. doi:10.1029/2012GL052014

Fasullo JT, Boening C, Landerer FW, Nerem RS (2013) Australia's unique influence on global sea level in 2010–2011. Geophys Res Lett 40:4368–4373. doi:10.1002/grl.50834

Fogt RL, Bromwich DH, Hines KM (2011) Understanding the SAM influence on the South Pacific ENSO teleconnection. Clim Dyn 36:1555–1576

Gill AE (1980) Some simple solutions for heat-induced tropical circulation. Q J R Meteorol Soc 106:447–462

Grainger S, Frederiksen CS, Zheng X (2013) Modes of interannual variability of Southern Hemisphere atmospheric circulation in CMIP3 models: assessment and projections. Clim Dyn 41:479–500. doi:10.1007/s00382-012-1659-7

Hartmann DL, Klein Tank AMG, Rusticucci M, Alexander LV, Brönnimann S, Charabi Y, Dentener FJ, Dlugokencky EJ, Easterling DR, Kaplan A, Soden BJ, Thorne PW, Wild M, Zhai PM (2013) Observations: atmosphere and surface. In: Stocker TF, Qin D, Plattner G-K, Tignor M, Allen SK, Boschung J, Nauels A, Xia Y, Bex V et al (eds) Climate change 2013: the physical science basis. Contribution of working group I to the fifth assessment report of the intergovernmental panel on climate change

Hendon HH, Thompson DWJ, Wheeler MC (2007) Australian rainfall and surface temperature variations associated with the Southern Hemisphere annular mode. J Clim 20:2452–2467

Hendon HH, Lim E-P, Liu G (2012) The role of air-sea interaction for prediction of Australian summer monsoon rainfall. J Clim 25:1278–1290

Hendon HH, Lim E-P, Arblaster J, Anderson DTL (2014a) Causes and predictability of the record wet spring over Australia in 2010. Clim Dyn 42:1155–1174. doi:10.1007/s00382-013-1700-5

Hendon HH, Lim E-P, Ngyuen H (2014b) Variations of subtropical precipitation and circulation associated with the southern annular mode. J Clim 27:3446–3460

Hope P, Lim E-P, Wang G, Hendon HH, Arblaster JM (2015) Contributors to the record high temperatures across Australia in late spring 2014. Bull Am Meteorol Soc 96(12):S149–S153

Huang B, Banzon VF, Freeman E, Lawrimore J, Liu W, Peterson TC, Smith TM, Thorne PW, Woodruff SD, Zhang H-M (2015) Extended reconstructed sea surface temperature version 4 (ERSST.v4). Part I: upgrades and intercomparisons. J Clim 28:911–930

Hudson D, Alves O, Hendon HH, Wang G (2011) The impact of atmospheric initialisation on seasonal prediction of tropical Pacific SST. Clim Dyn 36:1155–1171

Hurrell JW, Hack JJ, Shea D, Caron JM, Rosinski J (2008) A new sea surface temperature and sea ice boundary data set for the community atmosphere model. J Clim 21:5145–5153. doi:10.1175/2008JCLI2292.1.1

Jones DA, Wang W, Fawcett R (2009) High-quality spatial climate data-sets for Australia. Aust Meteorol Oceanogr J 58:233–248

Kang S, Polvani LM, Fyfe JC, Sigmond M (2011) Impact of polar ozone depletion on subtropical precipitation. Science 332:951–954

Kidston J, Frierson DMW, Renwick JA, Vallis GK (2010) Observations, simulations, and dynamics of jet stream variability and annular modes. J Clim 23:6186–6199

Knutson TR, Zeng F, Wittenberg AT (2013) Multimodel assessment of regional surface temperature trends: CMIP3 and CMIP5 twentieth-century simulations. J Clim 26:8709–8743

Kociuba G, Power SB (2015) Inability of CMIP5 models to simulate recent strengthening of the walker circulation: implications for projections. J Clim 28:20–35

Kosaka Y, Xie S-P (2013) Recent global-warming hiatus tied to equatorial Pacific surface cooling. Nature 501:403–407

Kumar A, Jha B, L'Heureux M (2010) Are tropical SST trends changing the global teleconnection during La Nina? Geophys Res Lett 37:L12702. doi:10.1029/2010GL043394

L'Heureux ML, Thompson DWJ (2006) Observed relationships between the El Niño-Southern Oscillation and the extratropical zonal-mean circulation. J Clim 19:276–287

Langford S, Hendon HH (2013) Improving reliability of coupled model forecasts of Australian seasonal rainfall. Mon Weather Rev 141:728–741

Lewis SC, Karoly DJ (2015) 2015: Are estimates of anthropogenic and natural influences on Australia's extreme 2010-2012 rainfall model-dependent? Clim Dyn 45:679–695. doi:10.1007/s00382-014-2283-5

Lim E-P, Hendon HH (2015a) Understanding and predicting the strong southern annular mode and its impact on the record wet east Australian spring. Clim Dyn 44:2807–2824

Lim E-P, Hendon HH (2015b) Understanding the contrast of Australian springtime rainfall of 1997 and 2002 in the frame of two flavors of El Nino. J Clim 28:2804–2822

Lim E-P, Simmonds I (2009) Effect of tropospheric temperature change on the zonal mean circulation and SH winter extratropical cyclones. Clim Dyn 33:19–32

Lim E-P, Hendon HH, Hudson D, Wang G, Alves O (2009) Dynamical forecast of inter-El Niño variations of tropical SST and Australian spring rainfall. Mon Weather Rev 137:3796–3810

Lim E-P, Hendon HH, Rashid H (2013) Seasonal predictability of the southern annular mode due to its association with ENSO. J Clim 26:8037–8054

Limpasuvan V, Hartmann DL (1999) Eddies and the annular modes of climate variability. Geophys Res Lett 26:3133–3136

Lorenz DJ, Hartmann DL (2001) Eddy-zonal flow feedback in the southern hemisphere. J Atmos Sci 58:3312–3327

Lu J, Chen G, Frierson DMW (2008) Response of the zonal mean atmospheric circulation to El Niño versus global warming. J Clim 21:5835–5851

Luo J-J, Wang G, Dommenget D (2015) Why did CMIP5 models fail to reproduce the recent La Nina-like climate shift? Technical report, ENSO workshop, University of New South Wales, Sydney, 4–6 Feb 2015

Lyon B, DeWitt DG (2012) A recent and abrupt decline in the East African long rains. Geophys Res Lett 39:L02702. doi:10.1029/2011GL050337

Manabe S, Holloway J (1975) The seasonal variation of the hydrological cycle as simulated by a global model of the atmosphere. J Geophys Res 80:1617–1649

Marshall AG, Hudson D, Wheeler M, Alves O, Hendon HH, Pook MJ, Risbey JS (2013) Intra-seasonal drivers of extreme heat over Australia in observations and POAMA-2. Clim Dyn. doi:10.1007/s00382-013-2016-1

McBride JL, Nicholls N (1983) Seasonal relationships between Australian Rainfall and the Southern Oscillation. Mon Weather Rev 111:1998–2004

Meehl GA, Teng H, Arblaster JM (2014) Climate model simulations of the observed early 2000s hiatus of global warming. Nat Clim Change 4:898–902

Meneghini B, Simmonds I, Smith IN (2007) Association between Australian rainfall and the Southern Annular Mode. Int J Climatol 27:109–121

Meyers GA, McIntosh PC, Pigot L, Pook MJ (2007) The years of El Niño, La Niña and interactions with the tropical Indian Ocean. J Clim 20:2872–2880

Murphy BF, Pettre P, Simmonds I (2002) Effects of changing baroclinicity on the Southern Hemisphere extratropical circulation. Q J R Meteorol Soc 128:1807–1826

Nicholls N (2011) What caused the eastern Australia heavy rains and floods of 2010/11? Bull Aust Meteorol Oceanogr Soc 24:33–34

Oke PR, Schiller A, Griffin DA, Brassington GB (2005) Ensemble data assimilation for an eddy-resolving ocean model of the Australian region. Q J R Meteorol Soc 131:3301–3311

Pacanowski RC (1996) MOM2. Documentation, user's guide and reference manual. Technical report. GFDL Ocean Group technical report 3.2, 328 pp

Peixoto JP, Oort AH (1991) Physics of climate. American Institute of Physics, College Park, MD, 520 pp

Randel WJ, Held IM (1991) Phase speed spectra of transient eddy fluxes and critical layer absorption. J Atmos Sci 48:688–697

Rashid HA, Hirst AC (2015) Investigating the mechanisms of seasonal ENSO phase locking bias in the ACCESS coupled model. Clim Dyn. doi:10.1007/s00382-015-2633-y

Rayner NA, Parker DE, Horton E, Folland CK, Alexander LV, Rowell DP, Kent EC, Kaplan A (2003) Global analyses of sea surface temperature, sea ice, and night marine air temperature since the late nineteenth century. J Geophys Res 108(D14):4407. doi:10.1029/2002JD002670

Reynolds RW, Rayner NA, Smith TM, Stokes DC, Wang W (2002) An improved in situ and satellite SST analysis for climate. J Clim 15:1609–1625

Robinson WA (2006) On the self-maintenance of midlatitude jets. J Atmos Sci 63:2109–2122

Saji NH, Goswami BN, Vinayachandran PN, Yamagata T (1999) A dipole mode in the tropical Indian Ocean. Nature 401:360–363

Sandeep S, Stordal F, Sardeshmukh PD, Compo GP (2014) Pacific Walker Circulation variability in coupled and uncoupled climate models. Clim Dyn 43:103–117

Santer BD et al (2005) Amplification of surface temperature trends and variability in the tropical atmosphere. Science 309:1551–1556

Schiller A, Godfrey JS, McIntosh PC, Meyers G, Smith NR, Alves O, Wang G, Fiedler R (2002) A new version of the australian community ocean model for seasonal climate prediction. CSIRO marine research report no. 240

Seager R, Harnik N, Kushnir Y (2003) Mechanisms of hemispherically symmetric climate variability. J Clim 16:2960–2978

Sen Gupta A, England MH (2007) Coupled ocean–atmosphere feedback in the southern annular mode. J Clim 20(3677–3692):2012. doi:10.1175/JCLI4200.1

Shi L, Hendon HH, Alves O, Luo J-J, Balmaseda M, Anderson D (2012) How predictable is the Indian Ocean Dipole? Mon Weather Rev 140:3867–3884

Smith TM, Reynolds RW, Peterson TC, Lawrimore J (2008) Improvements NOAAs historical merged land-ocean temp analysis (1880–2006). J Clim 21:2283–2296

Sobel AH, Held IM, Bretherton CS (2002) The ENSO signal in tropical tropospheric temperature. J Clim 15:2702–2706

Solomon A, Newman M (2012) Reconciling disparate twentieth-century Indo-Pacific ocean temperature trends in the instrumental record. Nat Clim Change 2:691–699

Stone PH, Carlson JH (1979) Atmospheric lapse rate regimes and their parameterization. J Atmos Sci 36:415–423

Su H, Neelin JD, Meyerson JE (2003) Sensitivity of tropical tropospheric temperature to sea surface temperature forcing. J Clim 16:1283–1301

Thompson DWJ, Wallace JM (2000) Annular modes in the extratropical circulation. Part I: month-to-month variability. J Clim 13:1000–1016

Trenberth KE, Fasullo JT (2012) Climate extremes and climate change: the Russian heat wave and other climate extremes of 2010. J Geophys Res 117:D17103. doi:10.1029/2012JD018020

Ummenhofer CC, Sen Gupta A, England MH (2015) How did ocean warming affect Australian rainfall extremes during the 2010/11 La Nina event? Geophys Res Lett 42:9942–9951. doi:10.1002/2015GL065948

Valke S, Terray L, Piacentini A (2000) The OASIS coupled user guide version 2.4. Technical report TR/CMGC/00-10, CERFACS

Vecchi GA, Clement A, Soden BJ (2008) Pacific signature of global warming: El Nino or La Nina? EOS Trans AGU. doi:10.1029/2008EO090002

Wang G, Alves O, Smith N (2005) BAM3.0 tropical surface flux simulation and its impact on SST drift in a coupled model. BMRC research report 107, 30 pp

White CJ, Hudson D, Alves O (2013) ENSO, the IOD and the intraseasonal prediction of heat extremes across Australia using POAMA-2. Clim Dyn. doi:10.1007/s00382-013-2007-2

Wilks DS (2005) Statistical methods in the atmospheric sciences. Academic Press, Cambridge

Xie P, Arkin PA (1996) Analysis of global monthly precipitation using gauge observations, satellite estimates, and numerical model predictions. J Clim 9:840–858

Xie S-P, Deser Clara, Vecchi Gabriel A, Ma Jian, Teng Haiyan, Wittenberg Andrew T (2010) Global warming pattern formation: sea surface temperature and rainfall. J Clim 23:966–986

Yin JH (2005) A consistent poleward shift of the storm tracks in simulations of 21st century climate. Geophys Res Lett 3:L18701. doi:10.1029/2005GL023684

Yin Y, Alves O, Oke P (2011) An ensemble ocean data assimilation system for seasonal prediction. Mon Weather Rev 139:786–808

Zhao M, Hendon H, Alves O, Yin Y, Anderson D (2013) Impact of salinity constraints on the simulated mean state and variability in a coupled seasonal forecast model. Mon Weather Rev 141:388–402

Zhao M, Hendon HH, Alves O, Liu G, Wang G (2015) Weakened El Niño predictability in the early 21st century. J Clim (submitted)